EUROPEAN ORGANIZATION FOR NUCLEAR RESEARCH

PERFORMANCE OF A MAGNETIZED TOTAL ABSORPTION CALORIMETER BETWEEN 15 GeV AND 140 GeV

M. Holder, J. Knobloch, J. May, H.P. Paar, P. Palazzi,
D. Schlatter, J. Steinberger, H. Suter, H. Wahl and E.G.H. Williams
CERN, Geneva, Switzerland

F. Eisele, C. Geweniger, K. Kleinknecht, G. Spahn and H.-J. Willutzki
Institut für Physik*) der Universität, Dortmund,
Fed. Rep. Germany

W. Dorth, F. Dydak, T. Flottmann, V. Hepp, K. Tittel and J. Wotschack
Institut für Hochenergiephysik*) der Universität, Heidelberg,
Fed. Rep. Germany

P. Bloch, B. Devaux, M. Grimm, J. Maillard, B. Peyaud,
J. Rander, A. Savoy-Navarro and R. Turlay
D.Ph.P.E., CEN-Saclay, France

F.L. Navarria
Istituto di Fisica dell'Università, Bologna, Italy

ABSTRACT

We have calibrated a magnetized iron-scintillator sandwich calorimeter in a hadron beam, finding an energy resolution equal to 16% FWHM at 140 GeV with 5 cm sampling. The hadron energy resolution (FWHM/mean) improves as $E^{-1/2}$ between 15 and 140 GeV. No effect due to the magnetic field was observed. Longitudinal and lateral shower containment were also investigated.

Geneva - 22 July 1977

(Submitted to Nuclear Instruments and Methods)

*) Supported by the Bundesministerium für Forschung und Technologie.

1. INTRODUCTION

Calorimetry[1] for high-energy electromagnetic radiation and hadron detection has become an increasingly popular technique in the past few years, along with the coming into operation of higher energy accelerators. A total absorption calorimeter, which measures the incoming particles' energy by sampling the ionization loss of the primaries and of the produced secondaries, has aspects complementary to a magnetic spectrometer. Its energy resolution improves with higher energies, it measures neutrals as well as charged particles, and it gives a response to the sum of the energies when hit by several particles. Total absorption detectors can therefore be usefully employed in the study of multiparticle final states, such as in deep inelastic lepton-induced reactions, or in large transverse momentum hadronic events, where the presence of neutral particles and the high multiplicity makes it difficult to carry out an individual-particle analysis which, in any case, is not always essential.

In the present paper we describe the response of a calorimeter consisting of iron-scintillator sandwiches to hadrons, muons and electrons with energies between 15 GeV and 140 GeV. The purpose of this calorimeter was to provide the hadron energy calibration in terms of pulse-height ratios between hadrons and muons for a neutrino counter experiment performed at CERN[2]. The design therefore follows closely that of the neutrino calorimeter, except that the over-all dimensions are smaller, such that the calorimeter can be easily installed in a test beam.

This report is subdivided as follows: a description of the test set-up is given in Section 2. The calibration with high-energy muons and the analysis of the data are described in Section 3. Section 4 gives an account of the results obtained with hadrons: the energy calibration and the resolution for 5 cm and 15 cm iron samplings, the longitudinal and lateral hadron shower distributions, and the effect of the magnetic field on the energy measurement.

2. DESCRIPTION OF THE TEST CALORIMETER SET-UP

The test calorimeter (Fig. 1) consists of 30 iron plates, each 120×120 cm^2 in area, sandwiched with 30 NE 110 plastic scintillator*) counters of dimensions $60 \times 80 \times 0.6$ cm^3 (S-counters). Since 3 cm thick iron plates were readily available, they were arranged in a periodic structure (6, 3, 6 cm thickness, repeated ten times), which is equivalent to 5 cm Fe samplings on the average. A copper coil was mounted on the calorimeter as shown in Fig. 1 in order to study the effect of the magnetic field on the energy calibration. The coil consists of 30 turns and is operated with a current of 200 A, producing a maximum field of 18 kG as measured with a pick-up coil. The total weight of the test calorimeter

*) Nuclear Enterprises Limited, Scotland.

is about 17 t and one third of it is used to study the response to incoming particles.

The S-counters are each connected via a fan-shaped plexiglas light-guide to a photomultiplier at one end (see Fig. 2). An aluminium-plexiglas mirror is glued at the end opposite the phototube to improve light-collection uniformity. The light attenuation of the S-counters was measured prior to installation in the calorimeter with a ^{106}Ru β source. Typical results are shown in Fig. 2: non-uniformities are at most 10% for a 20 cm region around the centre and this yields negligible corrections, owing to the limited lateral hadron shower development in iron (see Section 4.3).

NE 110 plastic scintillator counters, 45 × 5 × 0.6 cm^3 (L-counters), were inserted at depths of 30, 60 and 90 cm of iron, in order to study the radial shower development between 0 and 90 cm Fe. Six counters covered an area of 45 × 30 cm^2 on one side of the ideal beam line and a seventh one was installed 10 cm away on the other side to check the actual beam position (see Fig. 1).

Scintillator counters V, B_1, B_2, B_3, M_1, and M_2 are installed in the beam line as shown in Fig. 1. V is an anticounter with a 4 cm diameter hole in the centre, located 7.2 m in front of the calorimeter; B_1 and B_2 are two small beam-defining counters, 2 × 2 cm^2, set just in front of the calorimeter; B_3 is made larger, 8 × 8 cm^2, to increase the acceptance for muons; M_1 and M_2 are 35 × 35 cm^2 counters positioned behind a 1 m thick iron absorber after the calorimeter. The coincidence $\bar{V}\cdot B_1\cdot B_2\cdot B_3$ defines an incoming particle; muons used for calibration are signed by the coincidence $\bar{V}\cdot B_3\cdot M_1\cdot M_2$; electrons are separated up to $\sim$ 30 GeV from π^- by tagging with a differential Čerenkov counter located about 100 m upstream. The momentum acceptance of the beam was ±1%.

The photomultipliers used for the L- and S-counters are 32 mm diameter cathode, 10 stage 150 AVP*). They are operated at an average of -1.6 kV for the S-counters and of -1.4 kV for the L-counters via two independent power supplies: responses to muons are equalized within 20% by means of series resistors in the HV supply line. The last two dynodes of the S-counters' photomultipliers are supplied with booster voltage to eliminate a possible rate dependence. The beam intensity was kept low, i.e. no more than a few thousand hadrons in an 0.8 sec spill of the SPS. The light collected from the scintillators on the photocathode corresponds to about ten photoelectrons for a minimum ionizing particle. Under these operating conditions a muon traversing the S-counters gives a peak pulse height of about 5 mV on 50 Ω. The tubes are tested for linearity up to 300 mA, deviations from linearity are typically +5% at 200 mA, which corresponds to about 2000 equivalent muon traversals in a single scintillator, well above the range of pulse heights accepted in this experiment.

---

*) Philips, France.

The electronics used to process the phototubes' signals is the same as used in the neutrino experiment[2]. Each photomultiplier is connected to a 16-input, 12-output linear adder (of which only eight inputs are used). The input charge from each channel is split into three parts: 80% goes directly to an analogue-to-digital converter (ADC), 10% is mixed linearly with the other seven signals and is used for monitoring, 10% is mixed linearly with three other odd (or even) input signals and the total charge is sent to a separate ADC in order to enable the recovery from individual overflows. Because of the large dynamic range required in the experiment, the linear adders are provided with 30 dB amplifiers which are switched on when performing the calibration with muons.

The ADCs[2] have a linearly rising discharge current; the resulting quadratic response curve fits well the need of a large dynamic range, with moderate accuracy, in a hadron-shower-sampling calorimeter. A 100 MHz digitizing rate provides a resolution of ±0.25 pC for a maximum charge of 250 pC. Amplifier gain, signal splitting, and ADC characteristics are calibrated individually using a computer-controlled mercury pulse generator.

The data from the ADCs and from additional pattern units are stored in a 40-event, first in-first out (FIFO) buffer, and read out via CAMAC by a Nord-10 computer, which writes the output tape and provides monitoring information,

3. DATA ANALYSIS

3.1 Definition of an equivalent particle

Beam muons were used to calibrate the S-scintillators in terms of equivalent particle traversals. For each beam-energy setting two runs were taken: a "hadron" run with amplifiers switched off and a "muon" run with amplifiers on, in order to follow possible drifts in the characteristics of the electronics. A typical muon pulse-height spectrum is shown in Fig. 3. The peak of the muon spectra, corresponding to the most probable energy loss, defines one equivalent particle (ep). This peak value should be independent of the muon energy, since the most probable loss is not expected to vary with energy for energies above 10 GeV [3]. In the present experiment the peak position was found to be constant within 1% between 15 and 140 GeV: deviations are consistent with drifts in the electronics over the running period and with the accuracy in determining the peak values. The average muon energy loss, on the other hand, is expected to increase with energy owing to the increasing maximum momentum transfer in a single collision and to radiation losses[3,4].

A simple algorithm was found adequate to select the most probable pulse height, using the average pulse height:

$$\text{peak} = \text{mean} - 0.25 \times \text{standard deviation},$$

for counts above 50% of the maximum value, after smoothing the original distribution with a computer program[5]. We checked that this method agrees to about ±2% with peak fitting using Gaussian and Poisson distributions, and in fact this method yields a more stable response.

Since the hodoscope strips (L-counters) are not all reached by beam muons, they were calibrated independently with cosmic rays, correcting the measured peak values for the average angle of the cosmic rays.

The systematic uncertainty of the final energy calibration due to the definition of ep's and to the fitting of the ADC response is about 3%.

3.2 Hadron selection

Data were taken at 15, 30, 50, 75, 100, and 140 GeV with a negative beam consisting mostly of pions. As already mentioned, electrons were tagged at the lower energies (15 and 30 GeV) by means of a differential Čerenkov counter. At high energies electrons (or hadron cascades in which essentially all the energy goes into π^0's) were separated off-line by penetration and by pulse-height cuts on the first five S-counters. The fraction of electrons in the beam decreases with energy from about 5% at 30 GeV to about 1% at 75 GeV. Some data were collected with a 2.5 cm thick lead plate located 20 m in front of the calorimeter which eliminates the electron component in the beam.

The data were usually taken with the magnet current switched on, apart from a special test during which the calorimeter was demagnetized to check the effect of the magnetic field on the calorimeter response (see Section 4.2).

In order to simulate more closely the case of a neutrino interaction, where the vertex of the shower is known, we selected hadron showers starting at given depths in the calorimeter, using the cuts listed in Table 1. In addition, to obtain a clean sample, hadrons are required to interact between the second and the sixth iron plate. An additional cut in minimum penetration of the shower was introduced to get rid of some low-energy particles of short penetration. On the other hand, no cut was applied for hadron selection in the back of the calorimeter, unlike in the experiment of Engler et al.[6], where showers with a maximum penetration of 80 cm Fe were selected, possibly forcing a better energy resolution because of the reduced fluctuations in the shower development (see Section 4.4).

At higher energies, where the fraction of electrons in the beam is negligible, one can learn about backward-going particles (albedo) from a comparison with hadron showers starting in the first iron plate. Figure 4 shows the ratio between the total pulse heights observed for hadron showers initiating in plates 2 to 6 and for hadron showers initiating in plate 1. Showers starting deeper inside the calorimeter yield an $\sim$ 2.5% higher pulse height, independent of energy within errors between 50 and 140 GeV. This effect indicates backward-scattered particles which escape detection for showers starting in plate 1. The magnitude of the observed albedo is consistent with measurements at lower energies[7] and with the results of shower simulation[8]. In the following we will consider only hadron showers initiating in plates 2 to 6.

4. RESULTS

4.1 Energy calibration and resolution of the calorimeter

Spectra of hadrons and electrons observed with 5 cm average sampling at different energies are shown in Fig. 5. The distributions are well fitted by Gaussian functions with the parameters listed in Table 2 (statistical errors only). The mean number of equivalent particles measured in the calorimeter is plotted in Fig. 6a for hadrons and electrons as a function of the beam energy. A blown-up view of the energy calibration is shown in Fig. 7, where the number of equivalent particles (nep) per GeV is plotted versus the energy. Hadrons above 50 GeV are reasonably well described by the formula nep = 17.4 × E (GeV), whilst at 15 GeV the ratio nep/GeV is about 10% lower.

The electron calibration is given by nep = 18.5 × E (GeV), with a linear response within errors between 15 and 140 GeV. The observed π/e ratio varies from about 0.85 at the lowest energies to 0.94 at the highest energies. Whilst the electron calibration is linear, the visible fraction of hadron energy sampled in the calorimeter increases with energy, an effect which is expected on the basis of detailed shower simulation[9] (see Fig. 7). The absolute value of the electron energy, and therefore that of the π/e ratio, is subject to systematic uncertainties. First we recall that at high energy (75 and 140 GeV data) the electron identification is based only on shower development. In addition, since the beam transport vacuum pipe ended 60 m upstream from the test calorimeter, electrons radiated in the 0.2 radiation lengths of air. A bending magnet was inserted 30 m after the end of the vacuum pipe and selected electrons of slightly lower energy ($\sim$ 1 to 2%) compared to the nominal. Also, the electron-shower measurement depends on the response of only a few phototubes at the beginning of the calorimeter. Finally transition effects, due to the difference in the critical energies of the absorber and sensitive media, could lower by a few per cent the electron pulse height with respect to ideal sampling[10]. We estimate the total systematic error on the π/e ratio to be 5%.

The FWHM of the hadron and electron distributions divided by the mean is plotted in Fig. 6b as a function of the beam energy. The energy resolution for hadrons with 5 cm sampling is well described between 15 and 140 GeV by the formula

$$\frac{\text{FWHM}}{\text{mean}} = \frac{1.9}{\sqrt{E\ (\text{GeV})}} \qquad (5\text{ cm Fe, hadrons}). \tag{1}$$

This result compares well with the energy resolution obtained in previous experiments with iron-scintillator sandwich calorimeters[11], if one takes into account the effect of the different sampling thicknesses. With 5 cm sampling the energy resolution turns out to be about a factor of two better for electrons than for hadrons (see Table 2).

Electromagnetic showers develop in iron much more quickly than hadronic showers, owing to the ratio between the radiation length and the absorption length (~ 0.1). In principle, if the detector resolution in the beam direction is adequate, the π^0's produced in the first collision can be separated from the remainder of the hadron shower, and the fluctuations between showers of different π^0 content can be reduced. In order to study this effect we weighted the early pulse-height channels in the region of the electromagnetic shower development less than the subsequent channels, according to the relative average contributions of the two components. Using a weight equal to 0.85 for the pulse heights in the first six counters (30 cm Fe) after the shower start and to 1 for the rest, the energy resolution improves slightly: the contribution to the total FWHM/mean due to the fluctuations in the π^0 content of the individual showers is estimated to be about 5% at 140 GeV. Different weighting recipes, such as linearly increasing weights for the first six counters, yield the same results. This effect is hardly visible with the present sampling thickness (5 cm), but it indicates the possibility of some improvement in the energy resolution for thinner sampling and higher energies.

Data for hadrons with 15 cm sampling are obtained by summing up the pulse-heights from every third scintillator: the energy calibration and the resolution are shown in Figs. 8a and b respectively. The energy resolution follows the formula

$$\frac{\text{FWHM}}{\text{mean}} = \frac{3.6}{\sqrt{E\ (\text{GeV})}} \qquad (15\text{ cm Fe, hadrons}), \tag{2}$$

which is about 10% worse than the one expected from the results with 5 cm sampling assuming purely statistical fluctuations, i.e. Eq. (1) multiplied by $\sqrt{3}$.

To study possible systematic biases in the calorimeter response and in particular to study the effect of the photomultipliers' non-linearity at high charges, a special run was taken at 140 GeV beam energy with the S-counters high voltages

set to -1.4 kV. A difference in the hadron average response of (1.5 ± 0.5)% (statistical error) was found, which is well within our systematic uncertainties.

4.2 Effect of the magnetic field

The effect of the magnetic field on the calorimeter response was also investigated during a special run. The ratio between magnet-on and magnet-off (demagnetized) responses to hadrons of 30 GeV and 100 GeV is 0.995 ± 0.009 and 1.009 ± 0.006, respectively, where the quoted errors are statistical only. This test rules out a change in response due to the magnetic field bigger than 2% at the 90% confidence level. The observed energy resolutions are in the ratio 0.92 ± 0.05 at 30 GeV and 1.00 ± 0.06 at 100 GeV. Since again there is no systematic effect with beam energy, we can exclude a change in resolution due to the magnetic field bigger than 12% at the 90% confidence level. Moreover, no effect of the magnetic field was seen in the development of the shower.

Studies of magnetic-field effects on a calorimeter response for electromagnetic showers were also performed by Hitlin et al.[12], using a lead liquid-argon calorimeter: they found no detectable difference in the response to 1 GeV/c electrons for transversal fields up to 1.3 kG. Our measurements test magnetic field effects for ten times bigger fields in a ferromagnetic material, but with smaller field in the measuring device (scintillators) itself.

4.3 Longitudinal and lateral hadron shower development in iron

The mean number of equivalent particles in each counter and the corresponding r.m.s. fluctuations are given in Table 3 for each energy. The big fluctuations reflect the very different transition curves observed on an event-by-event basis. The average longitudinal hadron shower development is also represented in Fig. 9a. The data can be well reproduced, both in shape and absolute value, by a Monte Carlo simulation of the hadron cascade[13]. A simple parametrization of the form $t^{\alpha}e^{-\beta t}$ (where t is the depth in iron, and α and β are free parameters), in analogy with the parametrization of electromagnetic cascades, fails to reproduce the data near the shower maximum, where part of the incoming energy is transferred to π^0's and quickly dissipated. The exponentially falling part of the distributions corresponds to an absorption length ranging from 18.5 cm at 15 GeV to 28 cm at 140 GeV. Figure 9b shows the same distribution for electrons.

Some typical hadron shower parameters, namely the shower centre of gravity, the length corresponding to a 95% containment of the shower and the average shower length (defined as the length where the average particle number goes below one)

Table 1

Cuts for shower selection

(ph_i is the pulse height in scintillator i)

Beam energy (GeV)	Cut for conversion in plate i	Minimum number of counters with more than 3 ep
15, 30	ph_i, ph_{i+1} > 2.5 ep	5
50, 75	ph_i, ph_{i+1} > 5 ep	7
100, 140	ph_i, ph_{i+1} > 10 ep	9

Table 2

Results with 5 cm sampling

Nominal beam energy (GeV)	HADRONS mean (ep)	HADRONS σ (ep)	HADRONS FWHM / mean	ELECTRONS*) mean (ep)	ELECTRONS*) σ (ep)	π^-/e
15	234 ± 2	48 ± 2	0.479 ± 0.015	272 ± 3	26 ± 2	0.86 ± 0.02
30	496 ± 2	74 ± 2	0.347 ± 0.007	567 ± 4	43 ± 3	0.87 ± 0.02
50	865 ± 2	102 ± 1	0.275 ± 0.002	-	-	-
75	1326 ± 3	128 ± 2	0.227 ± 0.003	1376 ± 13	76 ± 11	0.96 ± 0.02
100	1725 ± 4	135 ± 2	0.183 ± 0.003	-	-	-
140	2449 ± 4	169 ± 2	0.162 ± 0.002	2598 ± 20	70 ± 17	0.94 ± 0.02

*) Note that the electron energy is somewhat lower than the hadron energy, and that at 75 and 140 GeV we have no unambiguous electron identification, see text.

Table 3

Mean number of equivalent particles
and r.m.s. fluctuation in each counter (hadrons)

Counter	15 GeV		30 GeV		50 GeV		75 GeV		100 GeV		140 GeV	
	mean	r.m.s.	mean	r.m.s.	mean	r.m.s.	mean	r.m.s.	mean	r.m.s.	mean	r.m.s.
1	19.0	21.0	22.1	33.1	51.1	51.6	52.4	60.3	91.6	76.7	96.1	89.5
2	31.8	31.9	46.1	53.2	94.6	72.8	114.0	91.9	166.1	99.4	201.7	139.3
3	37.0	27.9	72.9	53.3	140.2	83.6	196.0	104.8	260.1	125.6	341.8	182.7
4	31.7	23.9	70.3	47.6	118.4	68.4	186.0	100.3	223.0	107.7	314.1	143.4
5	26.7	19.3	61.8	41.9	101.6	59.2	160.3	82.8	185.4	84.1	267.4	121.9
6	20.3	22.1	48.1	38.7	76.8	53.7	122.4	74.7	145.8	81.5	228.0	117.0
7	16.0	16.0	35.2	35.7	58.8	50.4	87.6	62.0	112.5	75.5	175.8	102.8
8	12.6	14.7	27.2	27.4	44.9	38.0	70.5	53.8	88.6	63.5	138.1	82.1
9	8.4	13.7	19.4	21.4	32.5	32.1	52.8	43.2	73.4	61.2	107.3	74.8
10	6.7	12.3	17.1	21.7	27.6	30.0	51.4	48.0	65.4	59.4	99.4	76.9
11	5.6	11.3	15.2	21.2	23.0	28.0	40.7	40.6	50.8	48.4	80.4	65.9
12	4.4	9.0	12.2	19.9	20.5	28.4	37.6	42.7	44.5	46.2	73.0	69.8
13	2.9	6.4	9.4	17.0	15.5	24.9	28.6	35.2	36.1	43.0	54.6	59.5
14	1.9	4.6	7.3	15.1	13.3	22.0	25.0	30.9	34.5	45.5	50.2	56.9
15	1.6	4.4	6.9	15.0	10.8	20.0	20.8	28.4	23.9	32.6	43.5	55.2
16			5.3	13.8	8.1	17.6	17.2	27.7	20.8	30.7	34.1	44.5
17			5.3	13.3	7.7	20.4	15.3	27.9	19.5	29.2	31.4	44.5
18			4.1	10.6	6.2	14.2	13.9	24.7	14.7	26.3	28.1	43.0
19			2.7	6.7	5.4	15.2	10.7	24.0	11.0	22.0	21.5	40.9
20			2.0	4.9	4.4	13.1	9.3	20.1	10.9	23.4	17.3	32.9
21			1.6	4.2	4.2	12.2	7.0	13.5	8.8	19.3	17.6	34.2
22			1.2	4.5	2.3	9.4	5.2	16.1	6.6	15.2	12.2	29.7
23					2.1	8.3	3.9	11.9	5.2	12.9	10.8	24.7
24					1.2	4.3	3.5	12.1	4.6	13.2	8.6	22.4
25							3.3	11.6	4.0	13.8	8.0	21.2
26							2.4	10.4	3.1	10.3	6.3	19.7
27							1.4	4.8	2.1	7.4	4.5	15.8
28									1.8	7.2	4.2	17.4
29									1.5	6.8	3.2	12.3
30									1.1	5.2	2.4	10.6

REFERENCES

1. V.S. Murzin, *in* Progress in elementary particles and cosmic ray physics, vol. 9 (Eds. J.G. Wilson and S.A. Wouthuysen) (North-Holland, Amsterdam, 1967), p. 245.

2. M. Holder, J. Knobloch, A. Lacourt, G. Laverrière, J. May, H.P. Paar, P. Palazzi, F. Ranjard, P. Schilly, D. Schlatter, J. Steinberger, H. Suter, H. Wahl, E.G.H. Williams, F. Eisele, C. Geweniger, K. Kleinknecht, D. Pollmann, G. Spahn, H.J. Willutzki, W. Dorth, F. Dydak, V. Hepp, W. Heyde, K. Tittel, M. Výsočanský, J. Wotschack, P. Bloch, S. Bréhin, B. Devaux, M. Grimm, J. Maillard, Y. Malbequi, G. Marel, B. Peyaud, J. Rander A. Savoy-Navarro, G. Tarte, R. Turlay and F.L. Navarria, A detector for high-energy neutrino interactions, submitted to Nuclear Instrum. Methods.

3. R.M. Sternheimer and R.F. Peierls, Phys. Rev. B3 (1971) 3681.

4. C. Richard-Serre, CERN 71-18 (1971).

5. R. Brun, M. Hansroul, P. Palazzi and B. Peuchot, CERN DD/75/11 (unpublished).

6. J. Engler, W. Flauger, B. Gibbard, F. Mönnig, K. Runge and H. Schopper, Nuclear Instrum. Methods 106 (1973) 189.
   V. Böhmer, J. Engler, W. Flauger, H. Keim, F. Mönnig, K. Pack, H. Schopper, A. Babaev, E. Brachman, G. Eliseev, A. Ermilov, Yu. Galaktionov, Yu. Gorodkov, Yu. Kamishkov, E. Leikin, V. Lubimov, V. Shevchenko and O. Zeldovich, Nuclear Instrum. Methods 122 (1974) 313.

7. C.W. Fabjan and W.J. Willis, Proc. Calorimeter Workshop, FNAL, Batavia, 1975 (Ed. M. Atac), (FNAL, Batavia, 1975), p. 1.
   Cosmic ray measurements of particle albedo at high energy are reported by R.W. Ellsworth, J. Goodman, A. Ito, J. MacFall, F. Siohan, R.E. Streitmatter, S.C. Tonwar and G.B. Yodh, same Proc. p. 201.

8. T.A. Gabriel and W. Schmidt, Nuclear Instrum. Methods 134 (1976) 271.

9. A. Baroncelli, Nuclear Instrum. Methods 118 (1974) 445.

10. C.J. Crannell, H. Crannell, C.R. Gillespie, K. Pinkau and R.R. Whitney, Phys. Rev. 182 (1969) 1435, and references therein.

11. L.W. Jones, J.P. Chanowski, H.R. Gustafson, M.J. Longo, P.L. Skulic, J.L. Stone and B. Cork, Nuclear Instrum. Methods 118 (1974) 431.
    H. Whiteside, C.J. Crannell, H. Crannell, J.F. Ormes, M.J. Ryan and W.V. Jones, Nuclear Instrum. Methods 109 (1973) 375.
    B.C. Barish, J.F. Bartlett, A. Bodek, K.W. Brown, D. Buchholz, F. Jacquet, F.S. Merritt, F.J. Sciulli, L. Stutte, H. Suter, H.E. Fisk and G. Krafczyk, Nuclear Instrum. Methods 130 (1975) 49.
    D. Décamp, R. Lorenzi and W. Kienzle, private communication (1977).

12. D. Hitlin, J.F. Martin, C.C. Morehouse, G.S. Abrams, D. Briggs, W. Carithers, S. Cooper, R. DeVoe, C. Friedberg, D. Marsh, S. Shannon, E. Vella and J.S. Whitaker, Nuclear Instrum. Methods 137 (1976) 225.

13. P. Stähelin, private communication.
    A. Grant, Nuclear Instrum. Methods 131 (1975) 167.

14. L. Baum, H. Hilscher, F. Lobkowicz, C. Rubbia and A. Staude, Proc. Calorimeter Workshop, FNAL, Batavia, 1975 (Ed. M. Atac), (FNAL, Batavia, 1975), p. 295.

15. B. Friend, A. King, D. Kiss, W. Schmidt-Parzefall, K. Winter, F. Niebergall and W. Wilmsen, Nuclear Instrum. Methods 136 (1976) 505.

Figure captions

Fig. 1 : Top and front views of the magnetized calorimeter. The position of the L-counters used to measure the lateral shower development is indicated by the arrows.

Fig. 2 : Geometry of the S-counters superimposed with the response to minimum ionizing particles. The response in different regions of the scintillator is normalized to 1 at the position $x = y = 0$.

Fig. 3 : A typical pulse-height spectrum observed with beam muons. The arrow indicates the position of the most probable muon pulse height.

Fig. 4 : Ratio of pulse heights between showers starting inside the calorimeter and showers starting in the first iron plate.

Fig. 5 : Pulse-height spectra obtained with 5 cm average sampling at different beam energies. The solid histograms refer to negative pions and the dashed ones to electrons with Čerenkov tagging.

Fig. 6 : (a) Energy calibration and (b) energy resolution for 5 cm average sampling. The solid lines indicate the pion data behaviour and the dashed lines refer to electrons.

Fig. 7 : Expanded view of Fig. 6a. The calorimeter response is seen to be somewhat non-linear at low energy. The solid line is the best guess for a linear electron calibration. The dashed line shows the result of a Monte Carlo calculation of the calorimeter response to hadrons[9] normalized to 17.4 ep/GeV at 100 GeV.

Fig. 8 : (a) Energy calibration and (b) energy resolution for 15 cm sampling. The solid lines in (a) and (b) are scaled from the pion lines in Fig. 6, i.e. multiplied by $1/3$ and $\sqrt{3}$ respectively.

Fig. 9 : Longitudinal shower development in iron: (a) for π^--initiated showers; (b) for e^--initiated showers; the solid lines show fits to the e.m. shower development of the form $t^{\alpha} e^{-\beta t}$, where t is the depth in iron.

Fig. 10 : The shower centre of gravity, the length for 95% shower containment, and the shower length (see text), as a function of the π^- energy.

Fig. 11 : Shower centre-of-gravity distributions. The arrows indicate the average values.

Fig. 12 : Number of π^- which have not yet started a shower plotted as a function of the depth in iron. The solid lines correspond to a visible π^- interaction length of 19 cm.

Fig. 13 : Projected lateral shower distributions for hadrons integrated in depth between 0 and 90 cm.

Fig. 14 : Longitudinal and lateral shower development in iron: (a) 50 GeV; (b) 140 GeV.

Fig. 15 : Lateral dimension for 95% shower containment at each depth as a function of the depth in iron. The other dimension is fixed at ±22.5 cm by the size of the L-counters.

Fig. 16 : Hadron pulse-height spectra at 140 GeV: (a) without any software cut; (b) requiring no leakage at the end of the calorimeter ($ph_{30} < 1$ ep).

Fig. 17 : Effect of shower containment on the energy resolution. Data are shown at 75 and 140 GeV, without cuts and requiring no leakage (< 1 ep) at a given depth in the calorimeter. The point ▲ indicates the r.m.s. deviation in Fig. 16a, including the low pulse-height tail (the Gaussian fit of the peak is indicated by ●): no tails are observed in any of the other pulse-height spectra.

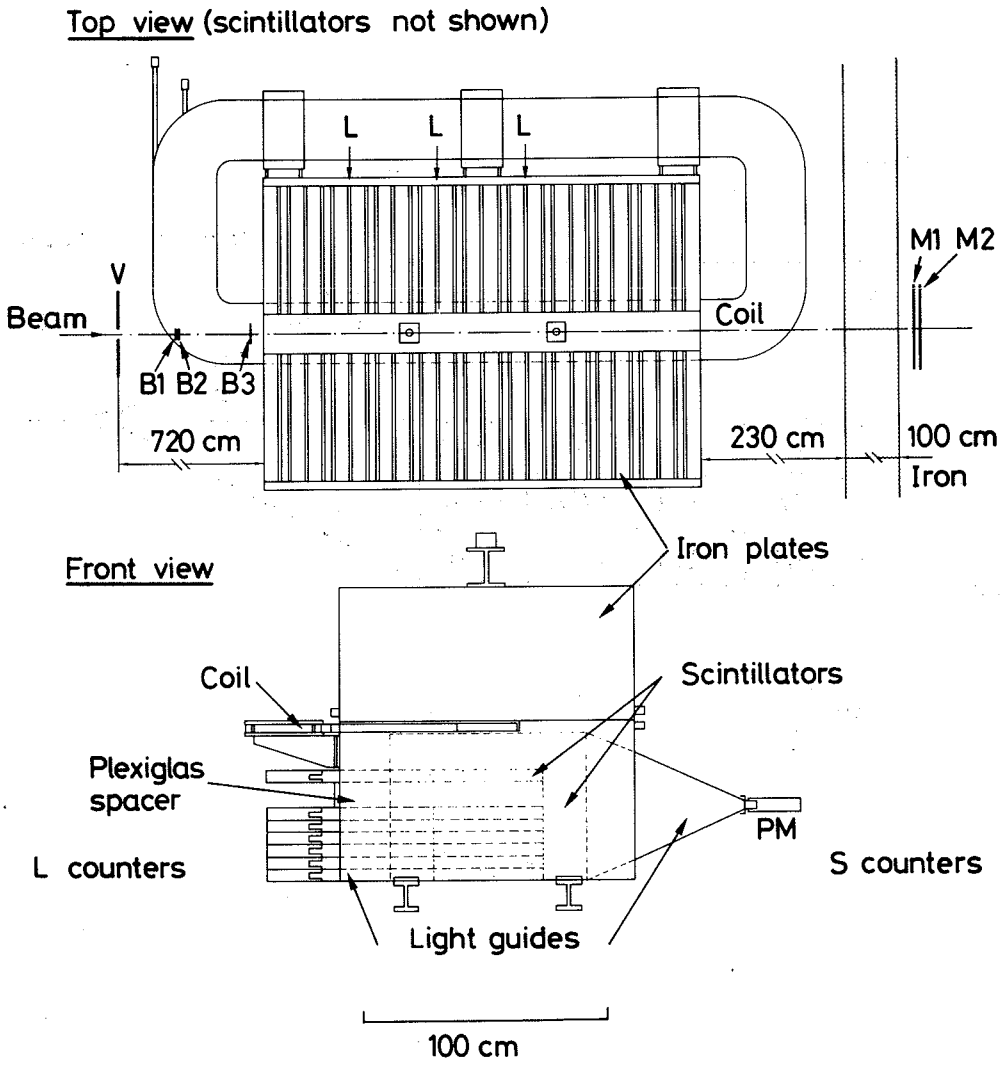
Top view (scintillators not shown)
L
L
L
M1 M2
V
Beam
Coil
B1 B2 B3
720 cm
230 cm
100 cm
Iron
Iron plates
Front view
Coil
Scintillators
Plexiglas
spacer
PM
L counters
S counters
Light guides
100 cm

Fig. 1

Counter S8

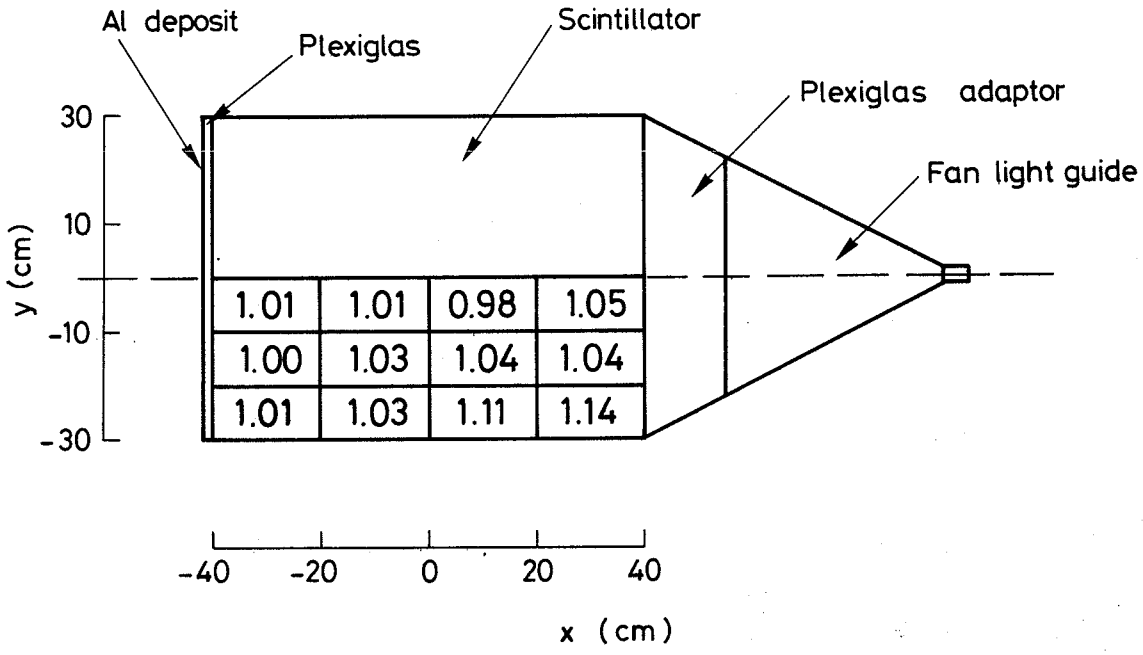

Fig. 2

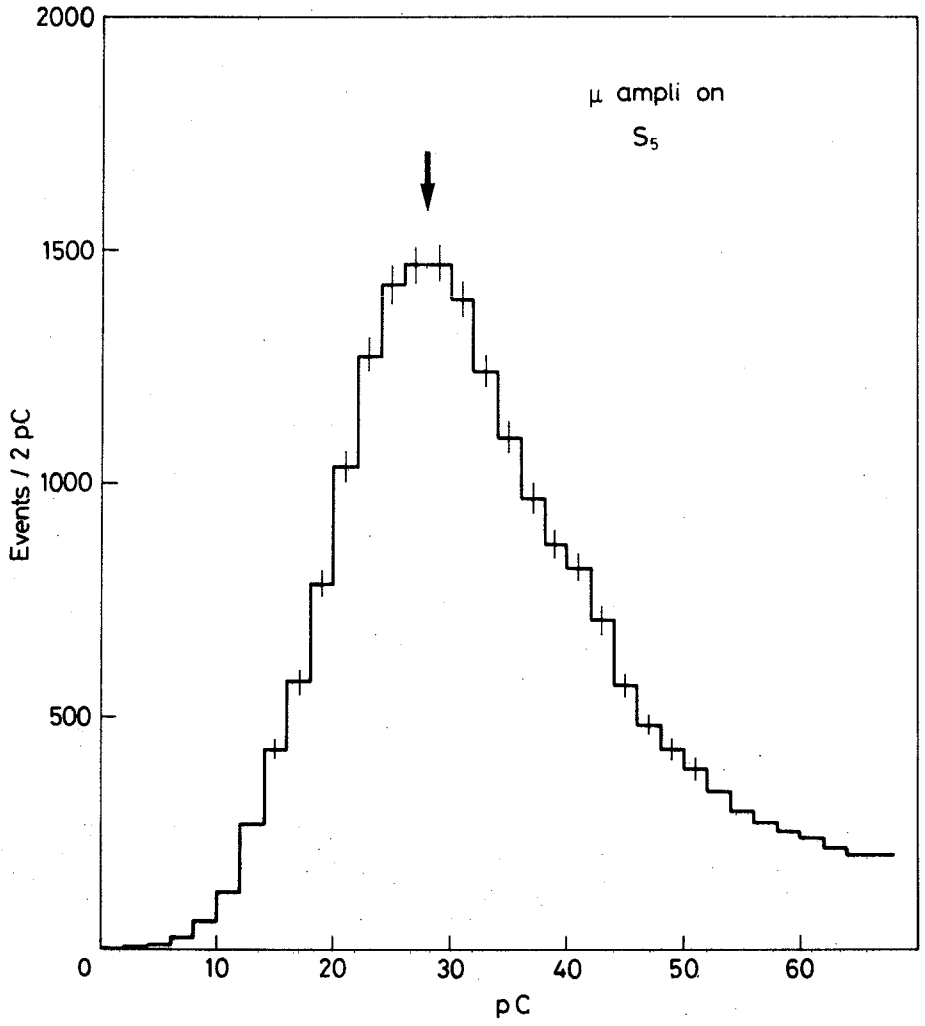

Fig. 3

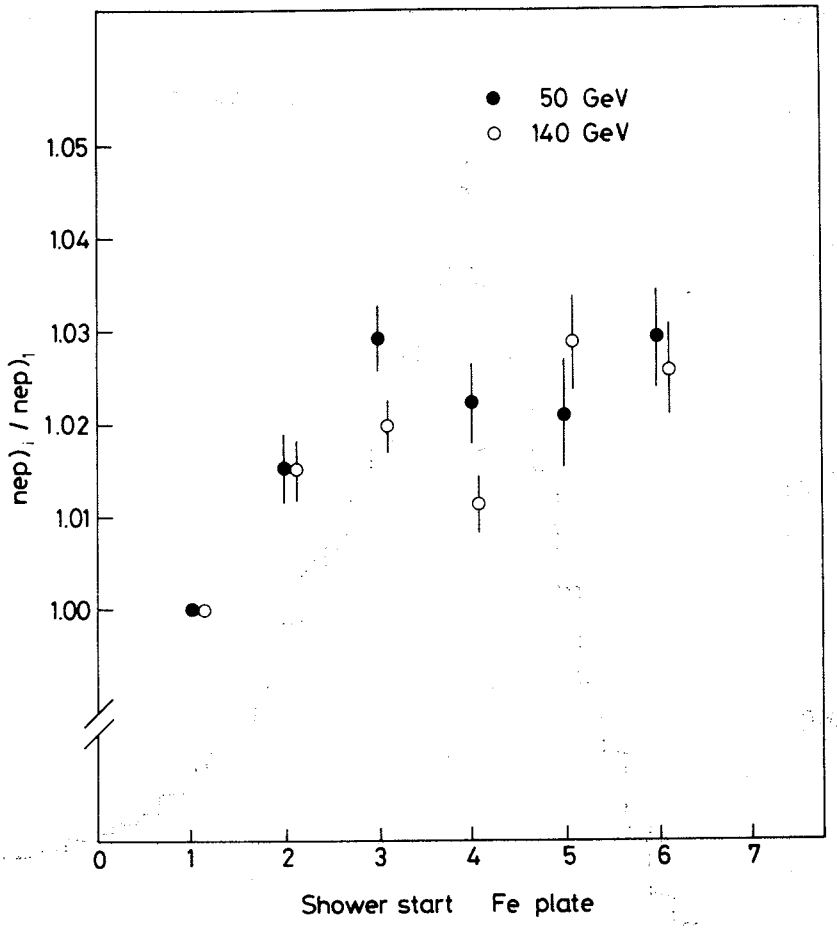
50 GeV
140 GeV
1.05
1.04
1.03
1.02
1.01
1.00
nep)$_i$ / nep)$_1$
0
1
2
3
4
5
6
7
Shower start Fe plate

Fig. 4

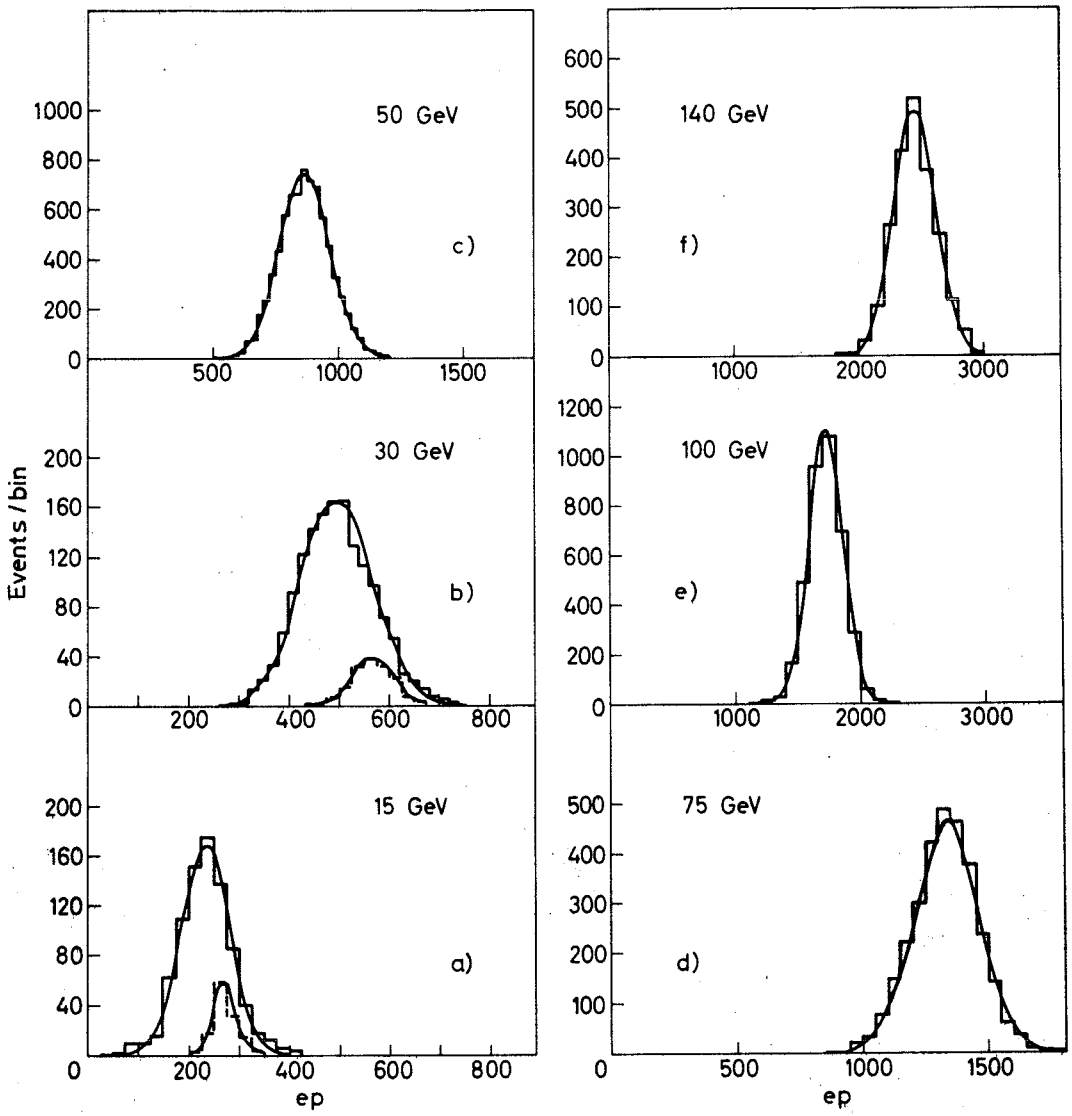
50 GeV
c)
30 GeV
b)
15 GeV
a)
140 GeV
f)
100 GeV
e)
75 GeV
d)
Events / bin
ep
ep

Fig. 5

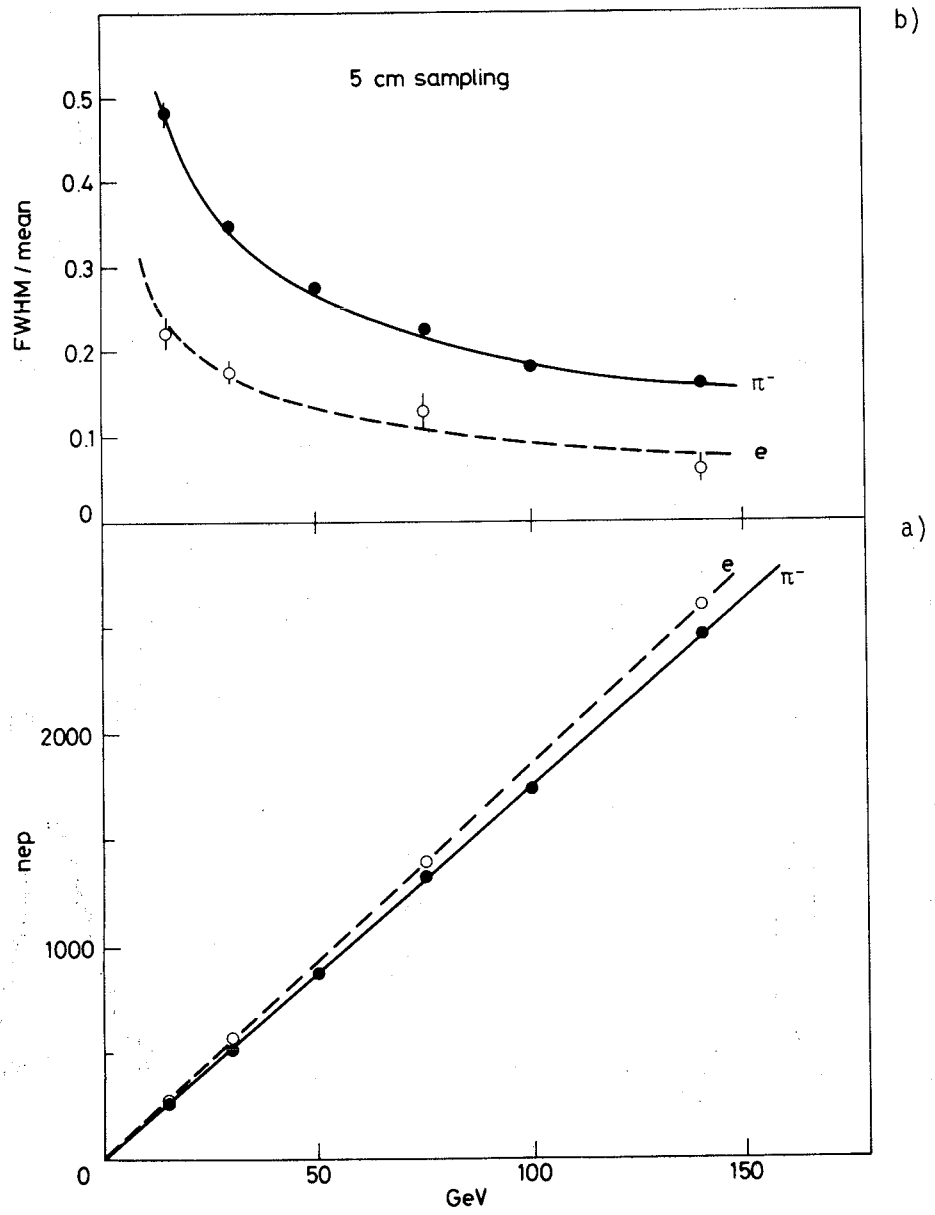
b)
5 cm sampling
FWHM / mean
0.5
0.4
0.3
0.2
0.1
0
π⁻
e
a)
e
π⁻
2000
1000
0
nep
50
100
150
GeV

Fig. 6

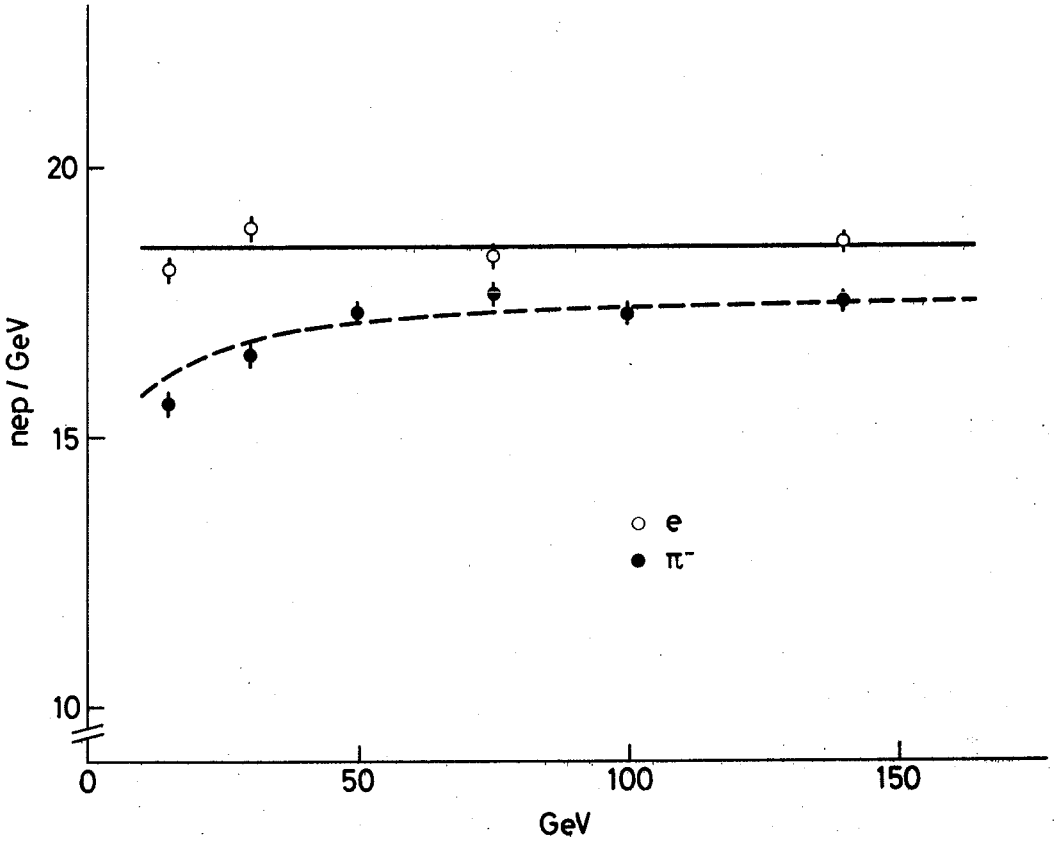

Fig. 7

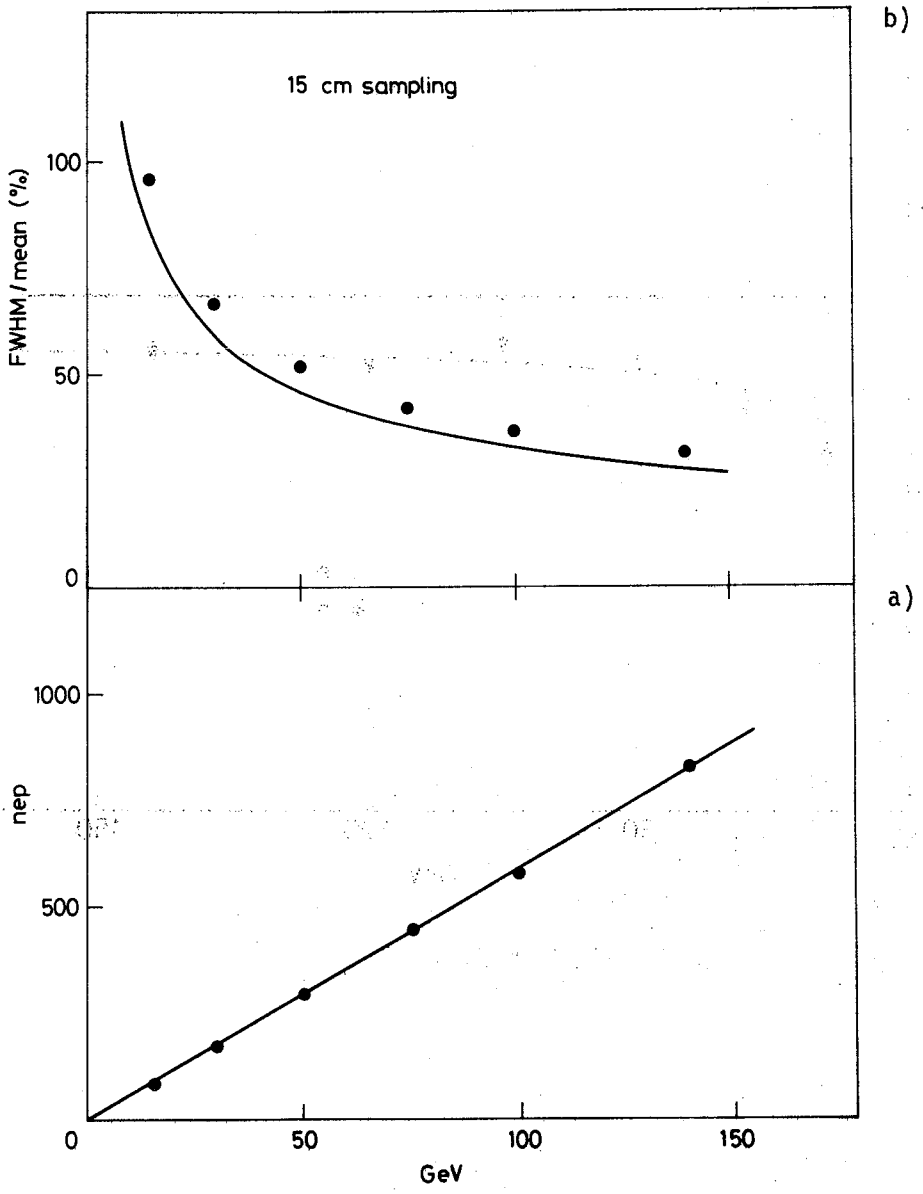
b)
15 cm sampling
FWHM / mean (%)
100
50
0
a)
1000
nep
500
0
50
100
150
GeV

Fig. 8

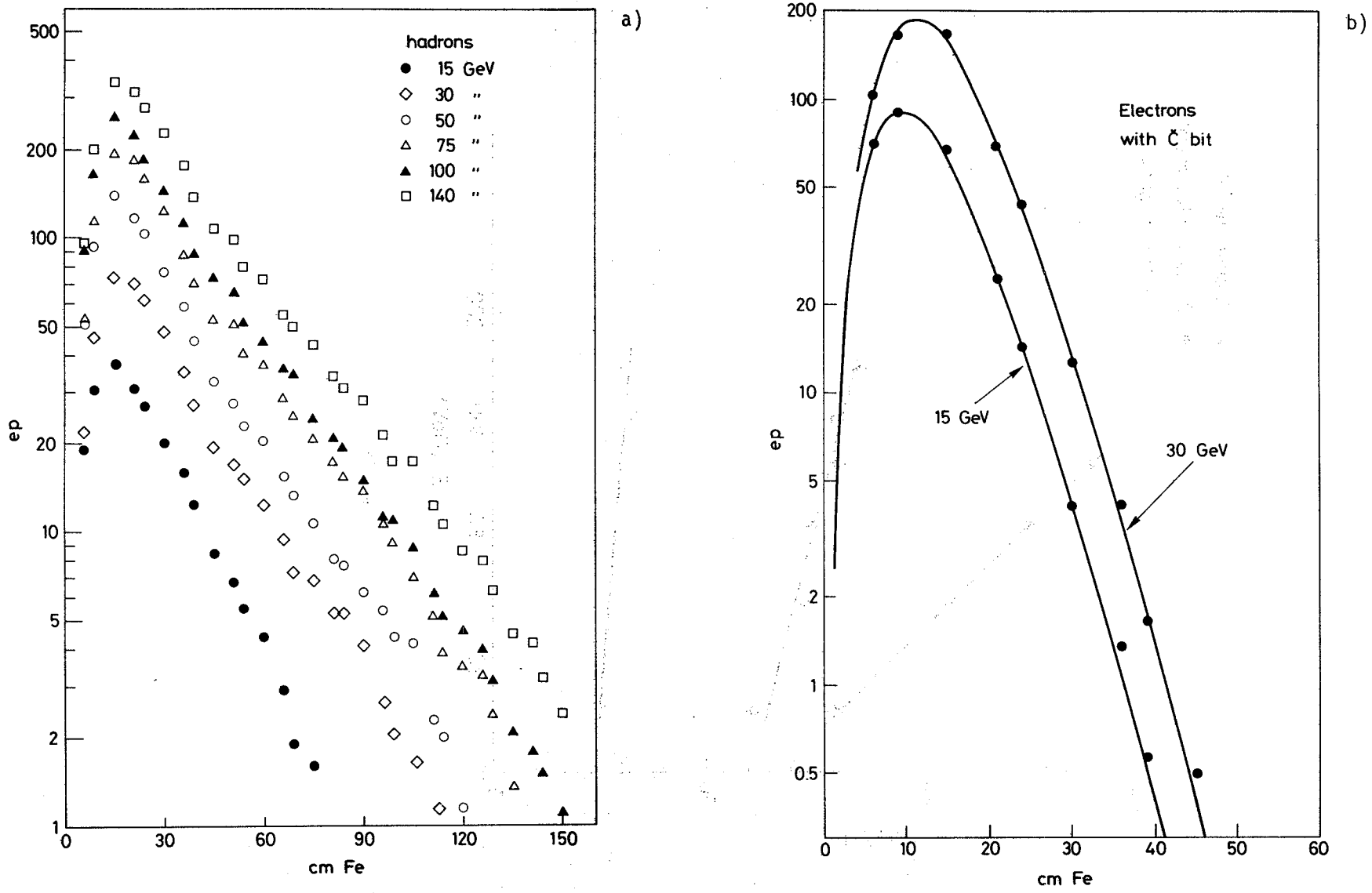
a)
hadrons
15 GeV
30 "
50 "
75 "
100 "
140 "
ep
cm Fe
b)
Electrons
with Č bit
15 GeV
30 GeV
ep
cm Fe

Fig. 9

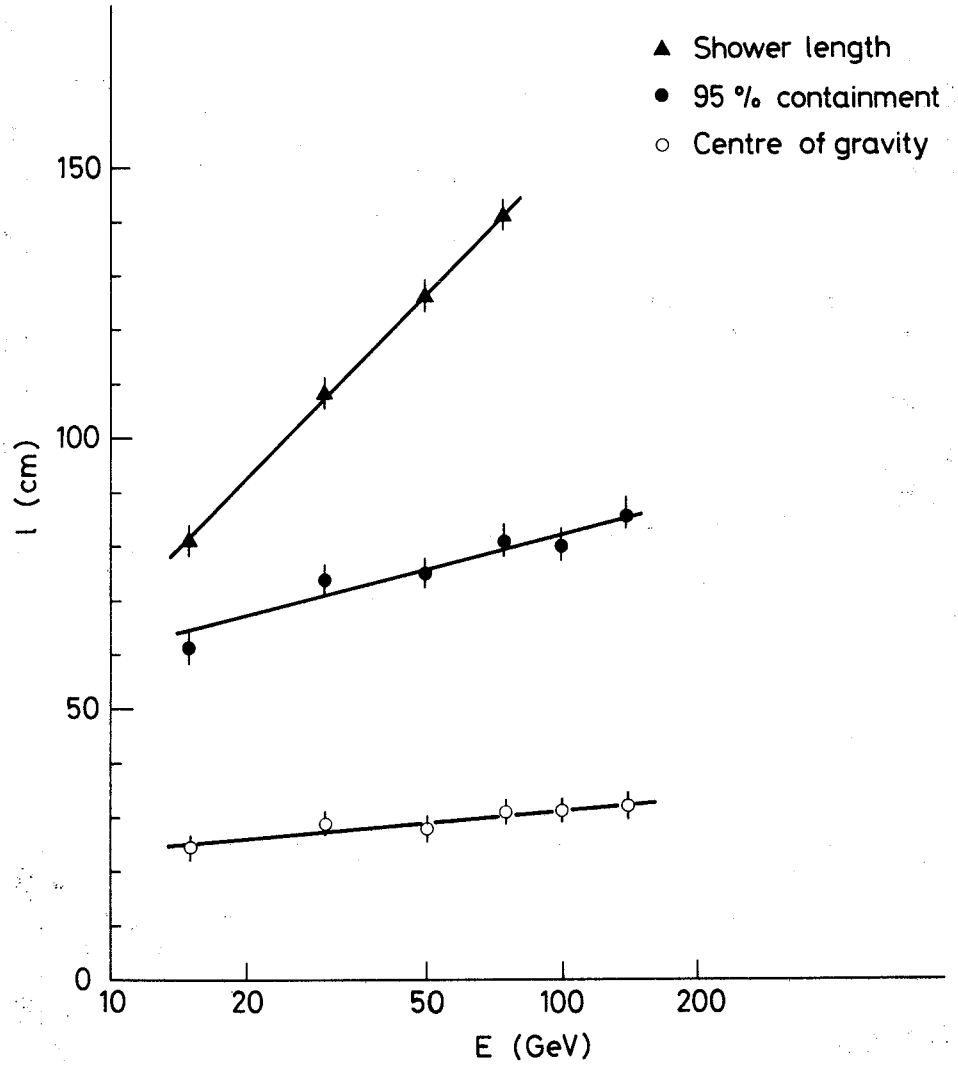
▲ Shower length
● 95 % containment
○ Centre of gravity
150
100
50
0
l (cm)
10
20
50
100
200
E (GeV)

Fig. 10

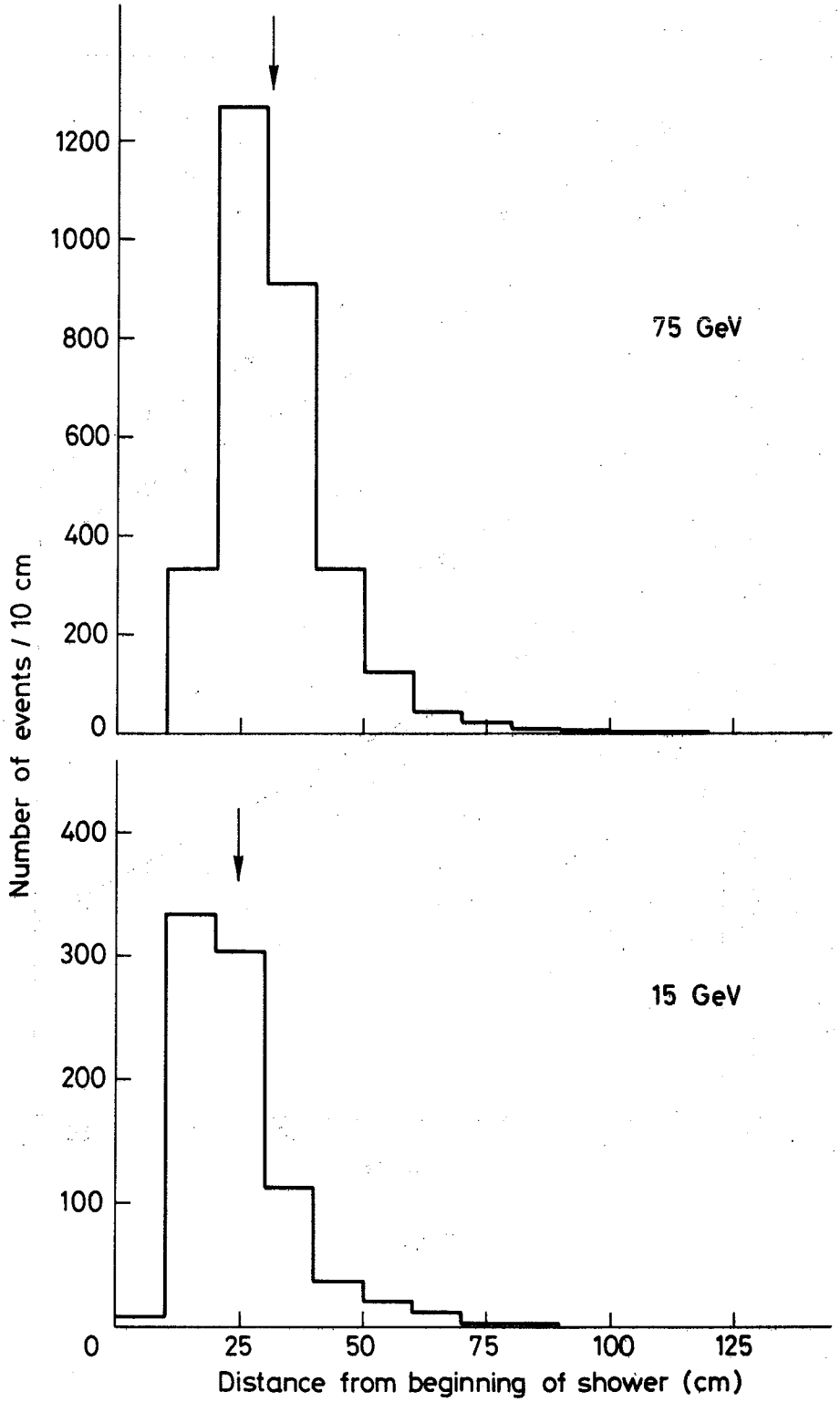
1200
1000
800
600
400
200
0
75 GeV
400
300
200
100
0
15 GeV
Number of events / 10 cm
25
50
75
100
125
Distance from beginning of shower (cm)

Fig. 11

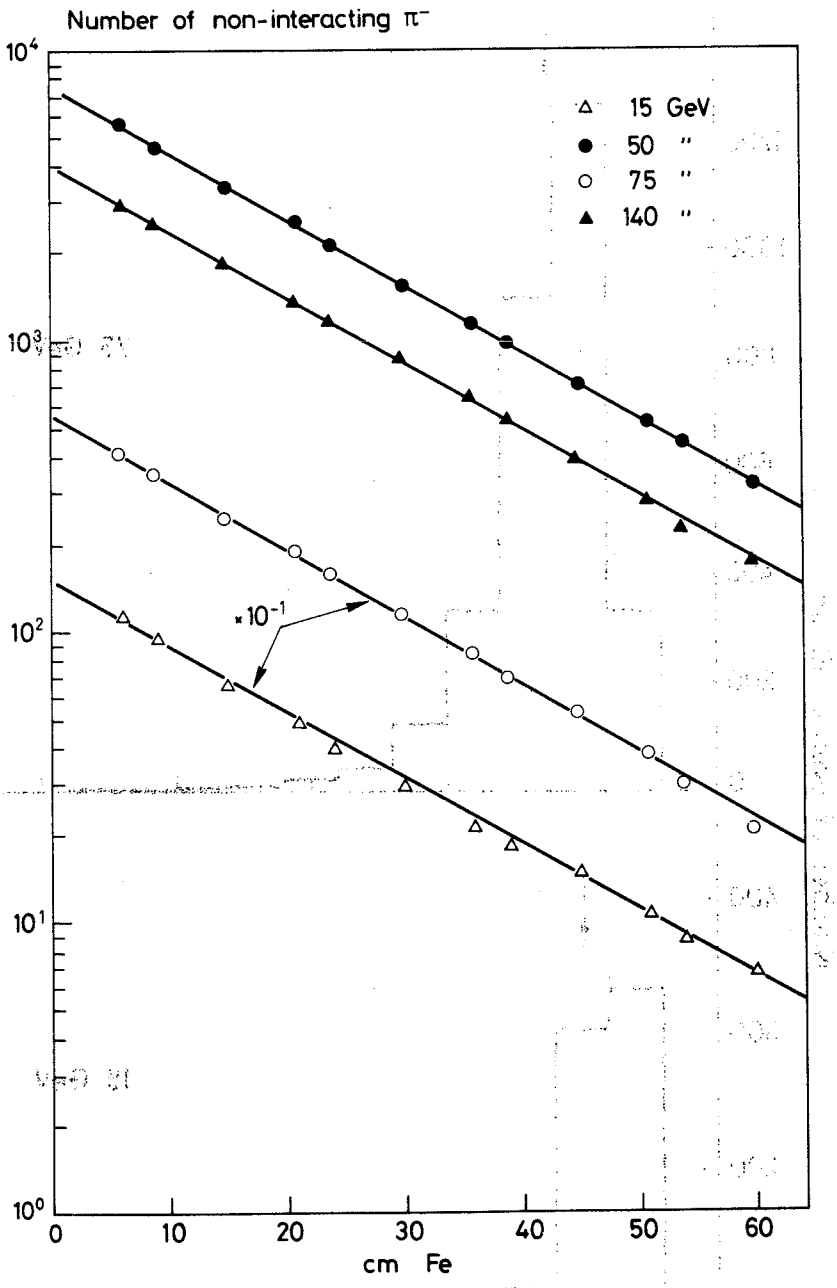

Fig. 12

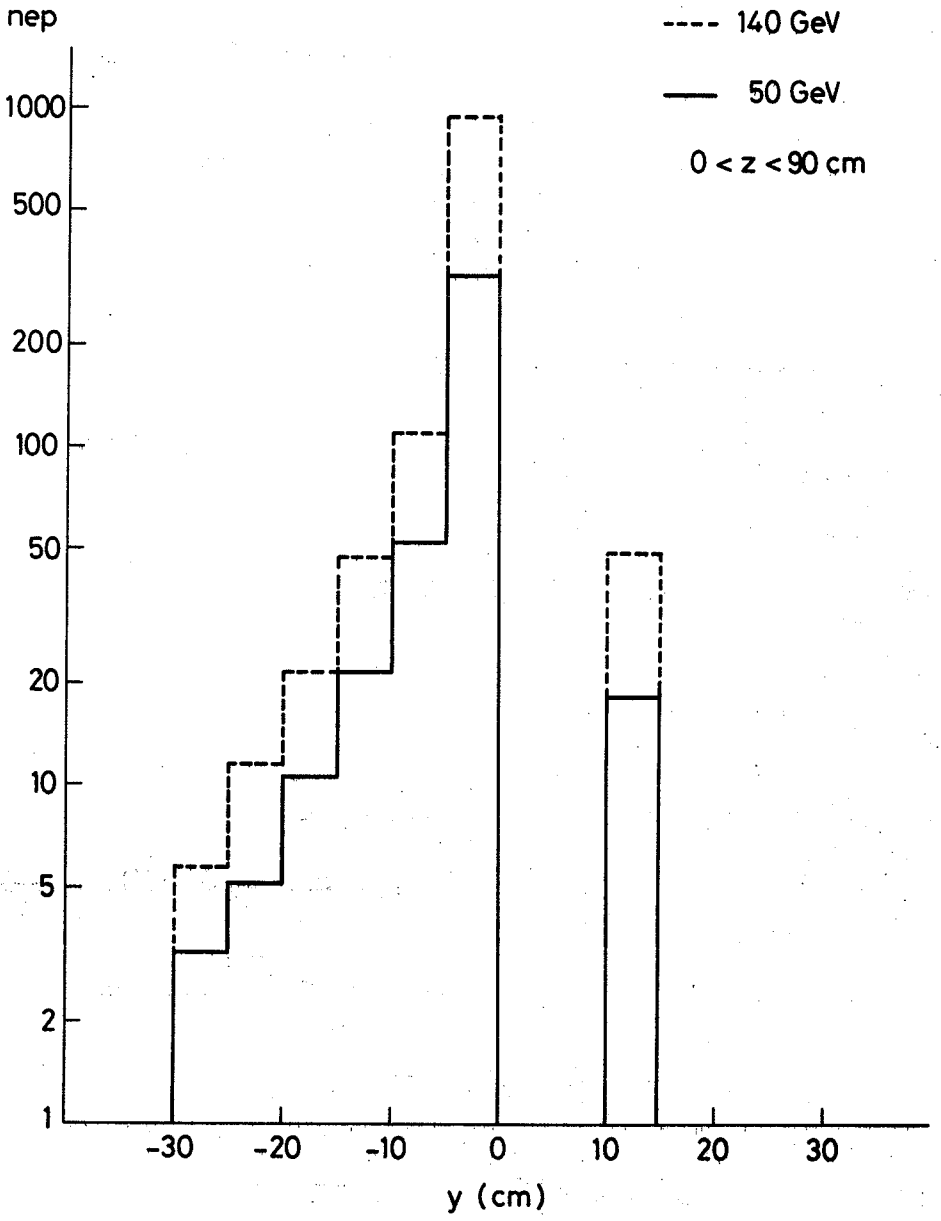
nep
---- 140 GeV
—— 50 GeV
0 < z < 90 cm
1000
500
200
100
50
20
10
5
2
1
-30
-20
-10
0
10
20
30
y (cm)

Fig. 13

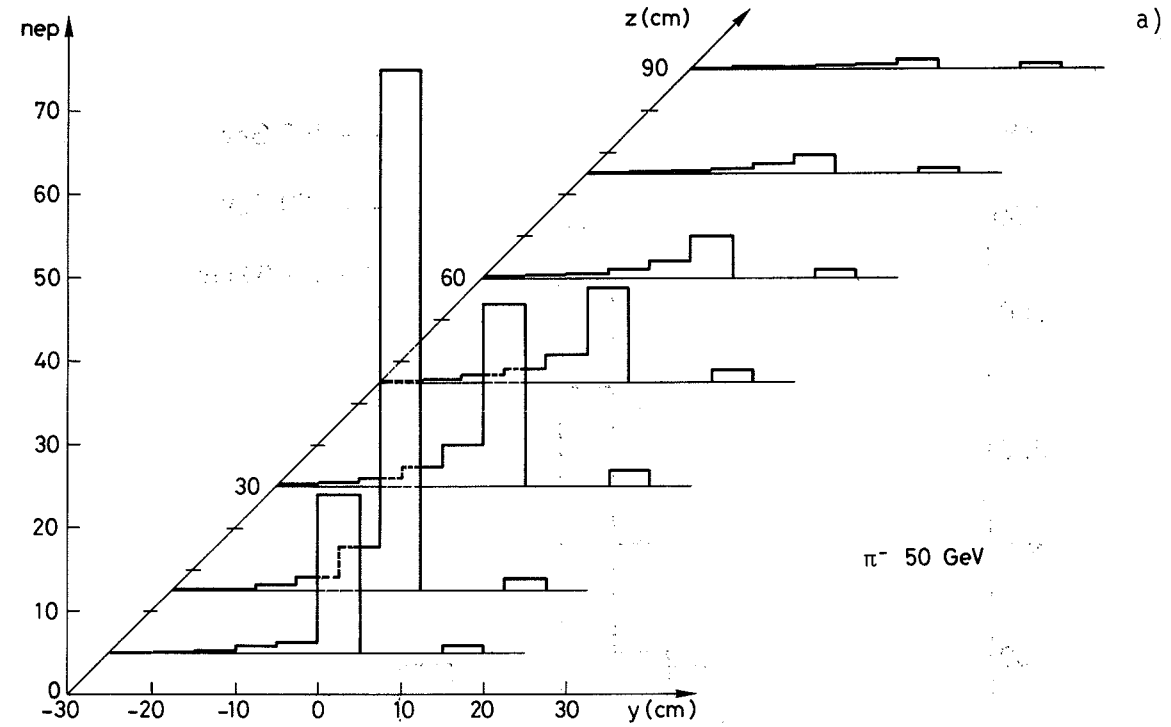
nep
z(cm)
a)
90
60
30
70
60
50
40
30
20
10
0
-30
-20
-10
0
10
20
30
y(cm)
π⁻ 50 GeV

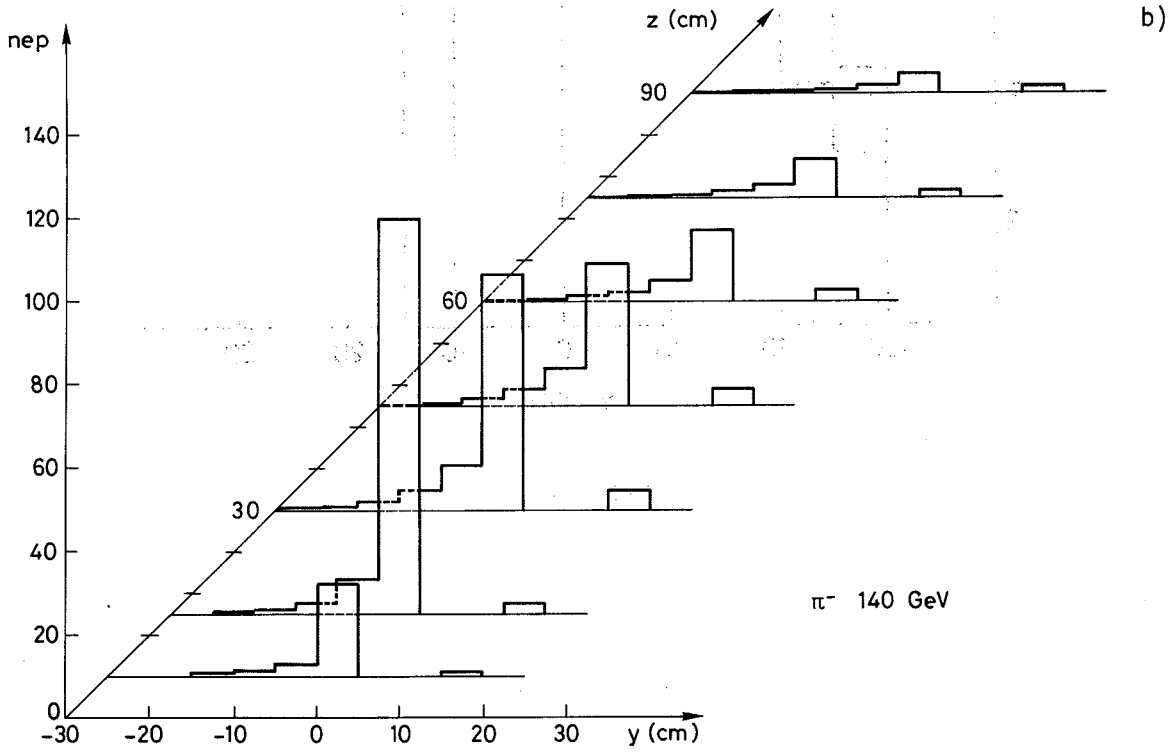
nep
z (cm)
b)
90
60
30
140
120
100
80
60
40
20
0
-30
-20
-10
0
10
20
30
y (cm)
π⁻ 140 GeV

Fig. 14

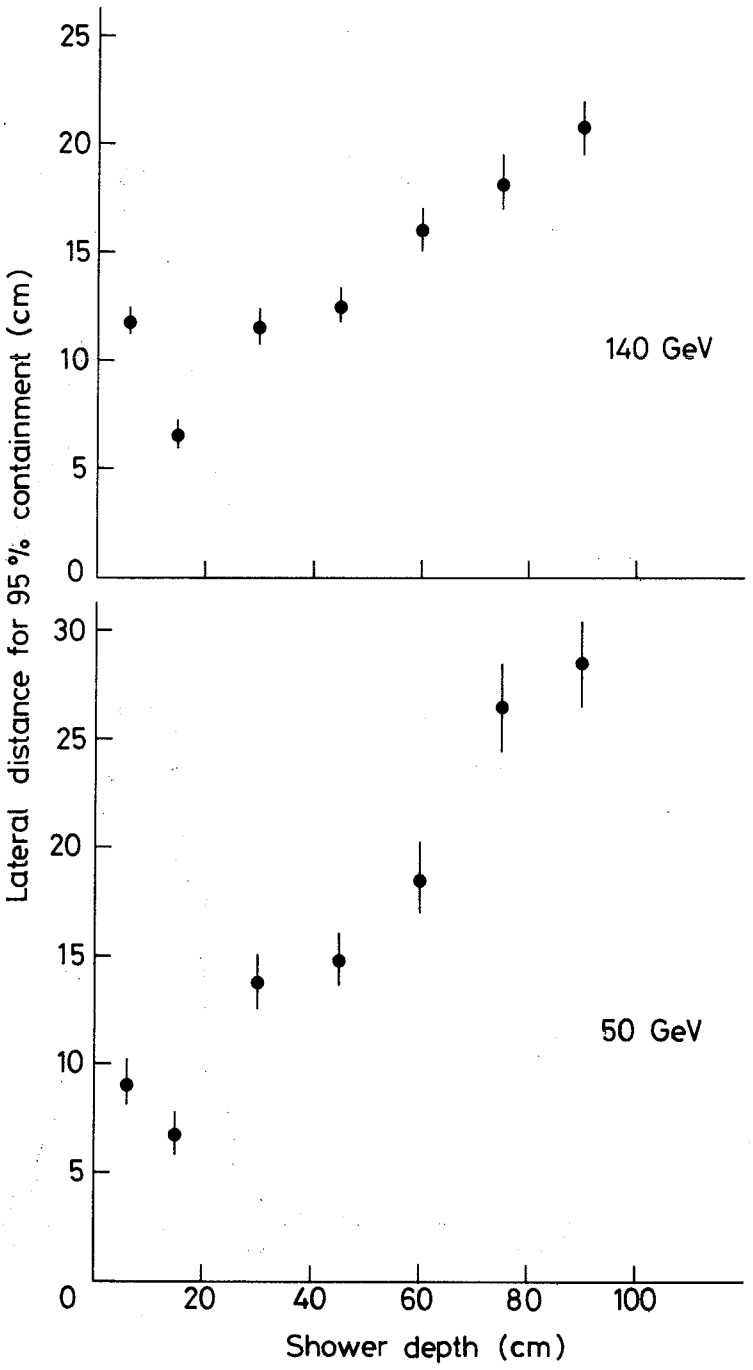
Lateral distance for 95 % containment (cm)
25
20
15
10
5
0
140 GeV
30
25
20
15
10
5
0
50 GeV
20
40
60
80
100
Shower depth (cm)

Fig. 15

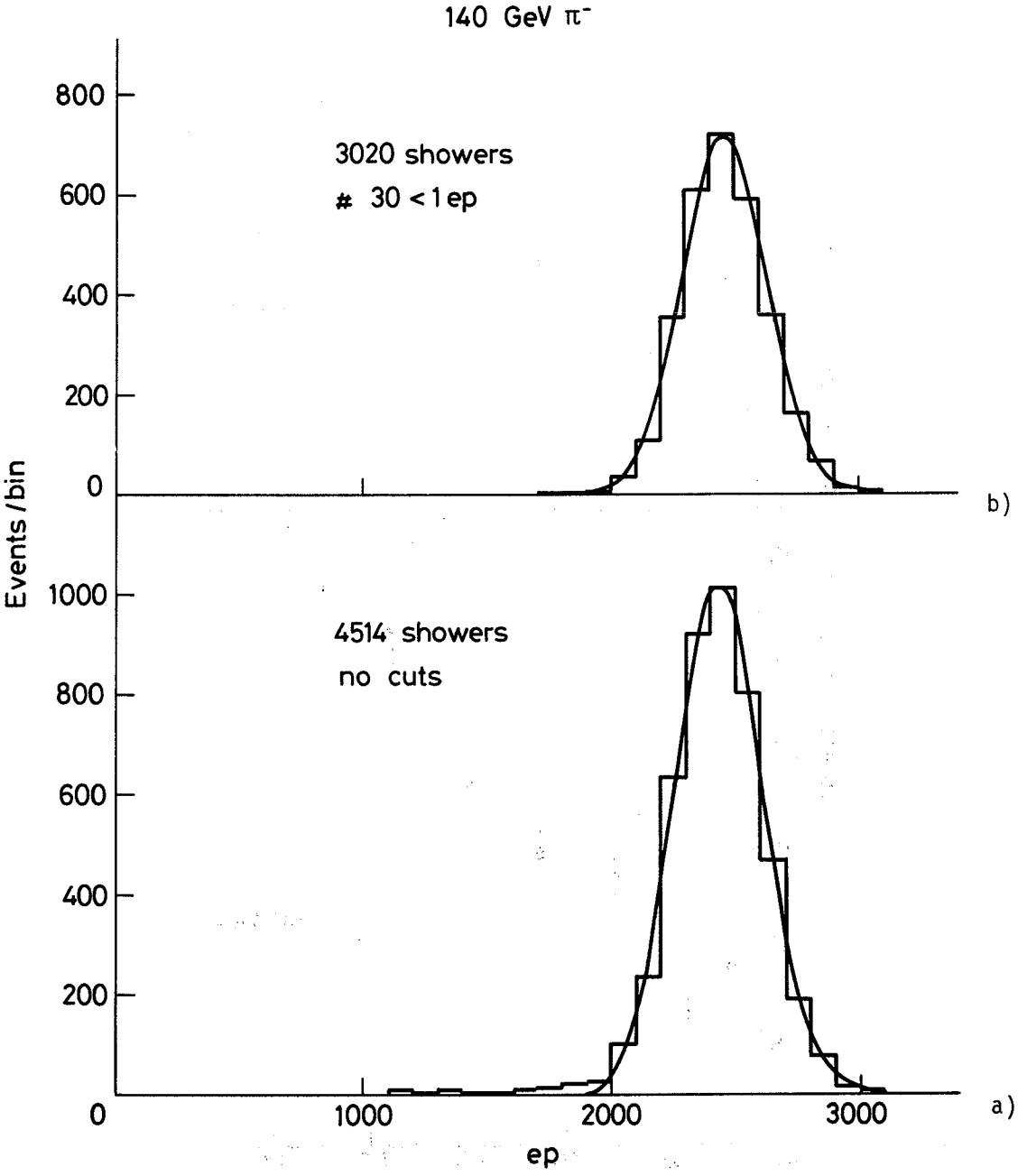
140 GeV π⁻
3020 showers
30 < 1 ep
4514 showers
no cuts
Events / bin
ep
b)
a)
0
200
400
600
800
1000
1000
2000
3000

Fig. 16

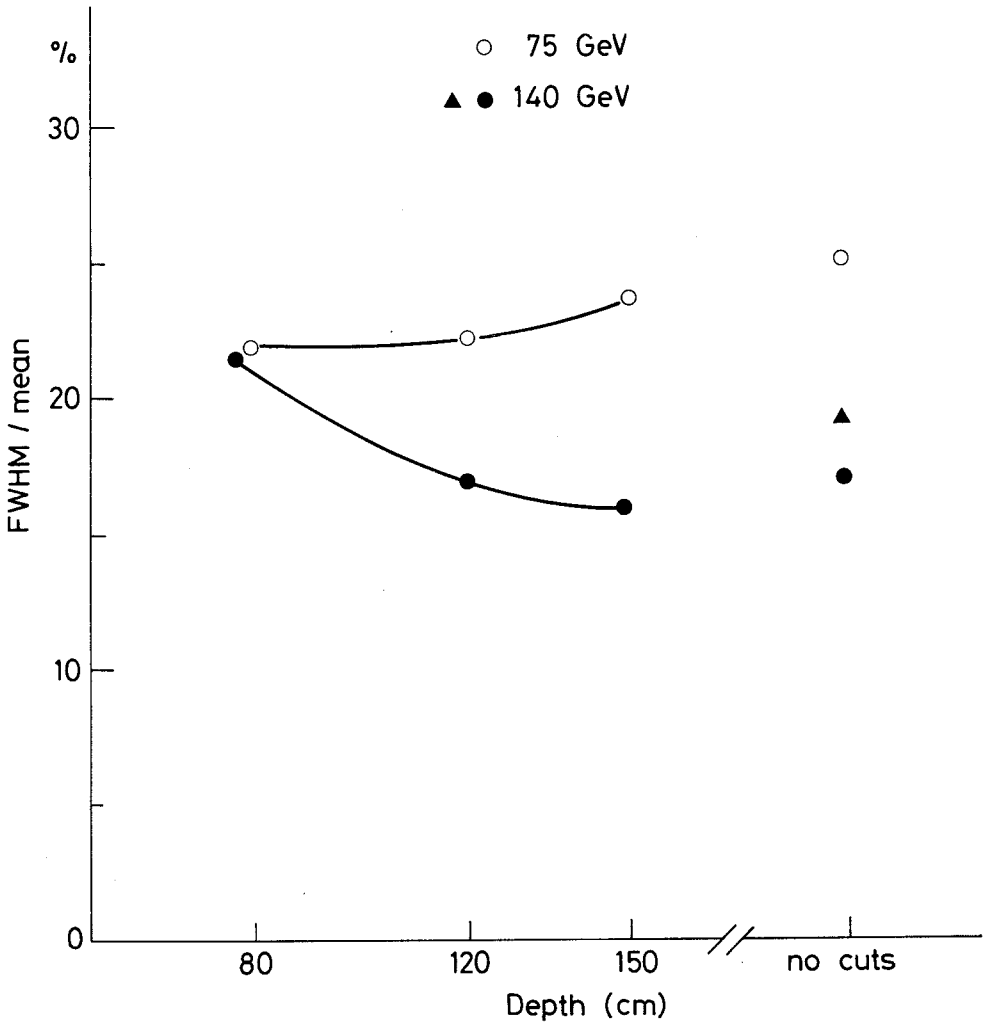

Fig. 17